Radar Interference Mitigation Using CNN Autoencoders with Spatial Attention

Idowu Ajayi, Wafa Njima

Radar Interference Mitigation Using CNN Autoencoders with Spatial Attention

Idowu Ajayi and Wafa Njima

ISEP, Institut Supérieur d'Electronique de Paris, 75006 Paris, France
Corresponding author: Idowu Ajayi (idowu.ajayi@isep.fr)

***Abstract*—As part of the growth in the automotive industry, there is an increase in the number of radar sensors that are deployed today. This growth comes at the cost of a potential increase in interference emanating from neighboring radar sensors that are within range. Traditionally, signal processing techniques have been used to mitigate interference but deep learning methods have drawn significant attention in recent times. To this end, we propose Radar-SACAE (Radar with Spatial Attention and Convolutional Denoising Autoencoder). This a deep learning model that applies spatial attention to the current range-doppler map input and previous inputs. This is then passed through a convolutional autoencoder to achieve very interesting performance, compared to existing models, in terms of signal-to-interference and noise ratio and error vector magnitude. This optimal performance is achieved with a highly significant reduction in computational complexity compared to that of other deep learning approaches.**

***Index Terms*—Autoencoders, convolutional neural networks, interference mitigation, FMCW radar, range-doppler map, spatial attention.**

I. Introduction and Motivations

Integrated Sensing and Communications (ISAC) has emerged as a key technology in fifth generation (5G) and beyond [1]. It opens the way for ground-breaking applications [2] such as Internet of Things (IoT), Robotics, and autonomous vehicles that require high-performance in sensing and communications. Due to the wide deployment of millimeter wave (mmWave) and massive Multiple-Input Multiple-Output (MIMO) technologies, communication signals in future wireless systems tend to have high-resolution in both time and angular domain, making it possible to enable high-accuracy sensing using communication signals such as radar sensing for automotive applications [3] such as blind-spot detection, collision-warning systems and self driving cars based on mmWave Frequency-Modulated Continuous Wave (FMCW) [4].

The mmWave FMCW radar can accurately measure the distance, azimuth, and velocity of a target thanks to its small size, low cost, and ability to be effective in most weather conditions. This is why it is a significant technology within the autonomous driving community. Several interference-mitigating signal processing techniques have already been implemented in the radars deployed in today's automobiles. However, with the increasing number of vehicles being equipped with radar sensors, and each vehicle having multiple radar sensors, the capability of radar systems to operate correctly in the presence of other radar systems in proximity is becoming a critical performance issue. As a result, radar-to-radar interference will increase dramatically and will be a significant challenge that the industry and researchers will have to address as a matter of urgency.

To mitigate interference, classical algorithms like Zeroing, Iterative Method with Adaptive Thresholding (IMAT) and Ramp filtering have been introduced [5], [6] and more sophisticated methods based on signal processing [7], [8]. Conventionally, these methods are based on a two-step process that detects and removes the interference. Thus, the removal performance heavily depend on the method used for interference detection. Moreover, the aforementioned methods can remove a part of the useful information in some circumstances. Therefore, Deep Learning (DL)-based methods have been introduced, outperforming traditional methods even under severe interference conditions. This is due to the fact that it directly processes the data and maintains the most useful signal. The majority of these methods deploy denoising autoencoders based on fully conventional networks. Taking into account the weight-sharing nature of convolution, many features of noise and interference are still retained in the denoised results. Almost all works do not consider the real-time performance and test the proposed models on simulated data. The authors in [9] proposed a denoising autoencoder that fuses both temporal and spatial information, outperforming both signal processing-based methods and conventional DL-based methods. However, this method is associated with considerable computational complexity. Our work aims to address the various problems faced by existing DL-based and non-DL-based methods for interference mitigation. The main contributions of this paper are summarized as follows:

- We propose a novel radar interference mitigation model that is based on spatial attention and a convolutional autoencoder.
- Our model is validated and tested using the real dataset provided by the authors in [9], [10].
- The proposed model outperforms other existing DL-based models with significantly reduced computational complexity.

The rest of this paper is organized as follows: Subsection II(A) is devoted to the principle of FMCW radar and in Subsection II(B), we describe the concept of radar interference. In Section III, we present our proposed Radar-SACAE model. The analysis methodology of the article is given in Section IV. Simulation results are discussed in Section V.

Finally, Section VI concludes the paper.

II. System Model

A. Principle of FMCW Radar

Radar systems work on the principle of sending out a radio signal and waiting for the echo. Compared to pulse radars, FMCW radars are more optimized for short ranges and are applicable in automotive and robotic applications, among others. In the type of FMCW radar considered, the radio frequency transmit signal is a chirp: a signal with a linearly ramping frequency. Hence, they are also referred to as chirp sequence (CS) radars. Figure 1 shows the frequency of the chirp as a function of time $f(t)$. It is dependent on the carrier frequency (f_{p}), the sweep bandwidth (B_{SW}), and the chirp duration (T_{p}) as given below:

$$f(t) = f_{\mathrm{p}} + \frac{B_{\mathrm{SW}}}{T_{\mathrm{p}}} t. \tag{1}$$

This transmit signal is reflected from targets in its view. This received signal is a time-delayed version of the transmit signal. It is then mixed with the transmit signal to form the so called Intermediate Frequency (IF) signal. The frequency of the IF signal is proportional to the amount of delay which is then used to calculate the range of the target. To calculate the velocity, the CS radar sends a quick sequence of chirps. The phase differences of the resulting IF signals is used to calculate the velocity of the target. The sequence of chirps is referred to as a frame.

As shown in Figure 1, the processing of the range and velocity information is done in two main steps. First, we have a fast-time FFT along the range dimension. This is followed by a slow-time FFT along the velocity dimension. The resulting two-dimensional image is is referred to as the Range-Doppler (RD) map which shows peaks that correspond to the range and velocity of the targets.

Assuming that a frame of IF signal consists of M chirps which each chirp having N samples, this will form the dimension of the RD matrix $M \times N$ where each point is given as $m \in M, n \in N$.

B. Concept of Radar Interference

Inspired by [11], there are two main types of interference in FMCW radar: Crossing and Parallel. Parallel interference occurs when the victim and the aggressor chirps have exactly the same slope. The effect of parallel interference is the so called ghost targets. Crossing interference, on the other hand, occurs when the victim and aggressor chirps have different slopes. The effect of the aggressor is visible only if their frequency difference falls within the IF bandwidth. The effects of crossing interference include an increase in the noise floor, reduction in the signal to noise ratio (SNR) of strong peaks, and possible coverage of weak peaks. This reduces detection probability and creates momentary blind spots.

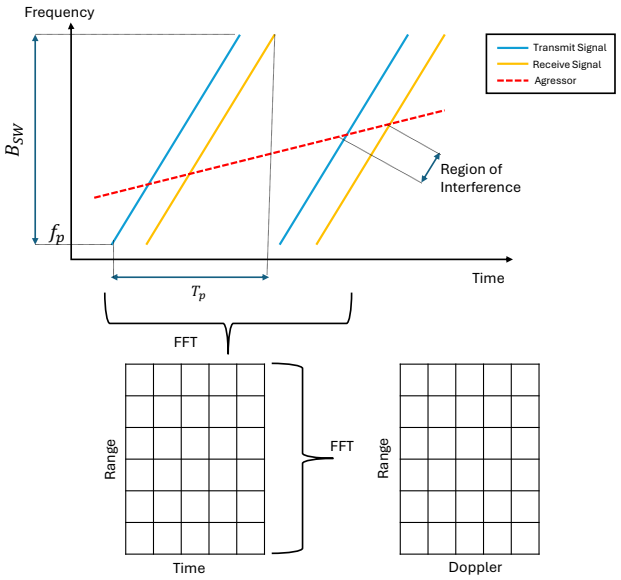

Fig. 1: Illustration of FMCW Radar with 2D FFT processing.

In the presence of interference, the corrupted IF signal is expressed as:

$$S_{\mathrm{IF(n,m)}} = \sum_{o=1}^{N_o} S_{O,o(n,m)} + \sum_{i=1}^{N_i} S_{I,o(n,m)} + v(n,m), \tag{2}$$

where n and m are the row and indices of the RD map, O is the set of target peaks, I is the set of interfered positions, and v is the AWGN. Without interference, the received power in FMCW radar in dBm is given as:

$$P_{\mathrm{rx}} = P_{\mathrm{tx}} + G_{\mathrm{tx}} + G_{\mathrm{rx}} + RCS - 10\log_{10}\left(\frac{(4\pi)^3 d^4}{\lambda^2}\right), \tag{3}$$

where P_{tx} is the transmit power, G_{tx}/G_{rx} are transmit antenna gain/receive antenna gain, RCS is the radar cross section, λ is the radio frequency wavelength, and d is the distance between transmit and receive antennas. When interference occurs, the received signal strength of an interfering radar in dBm is computed as:

$$P_{\mathrm{int}} = P_{\mathrm{tx}} + G_{\mathrm{tx}} + G_{\mathrm{rx}} - 10\log_{10}\left(\frac{4\pi d}{\lambda}\right)^2. \tag{4}$$

Comparing (3) to (4), it is clear that the effect of interference on the received power is highly significant. This means interference is likely to dominate, even when the aggressor is farther to the victim than the target. Indeed interference mitigation is very crucial in FMCW radar.

III. Radar-SACAE

Our proposed model is referred to as Radar with Spatial Attention and Convolutional Denoising Autoencoder (Radar-SACAE). It restores the victim radar by mitigating the interference in the RD map. This process is done in three main stages: Spatial Attention, Encoding, and Decoding.

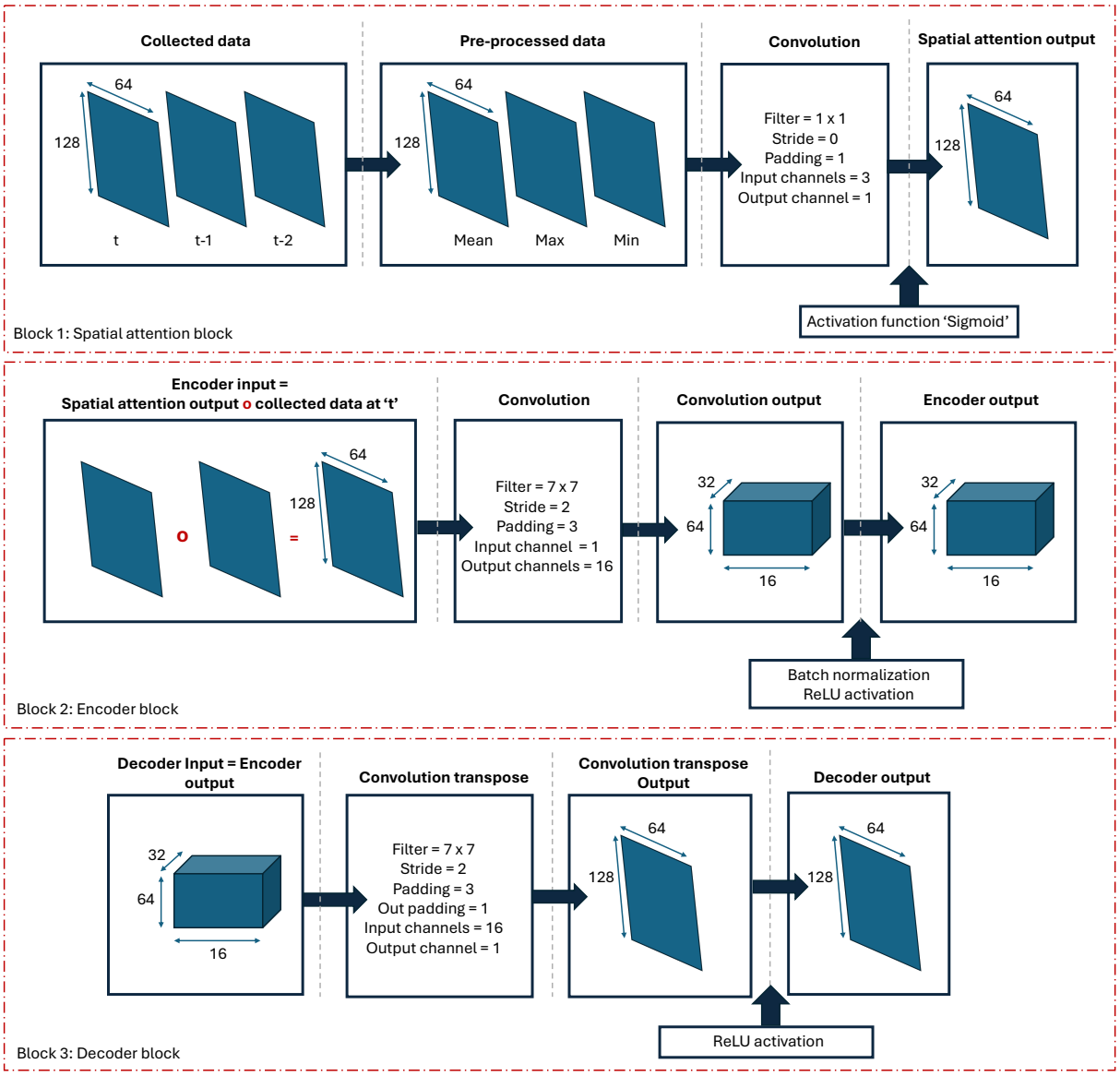

Fig. 2: The pipeline of the proposed Radar with Spatial Attention and Convolutional Denoising Autoencoder (Radar-SACAE).

A. *Spatial Attention*

The first operation in Radar-SACAE is the spatial attention. Spatial attention is a mechanism, popular in computer vision, used to give focus to certain parts or regions of the input image over others [12]. We realize that the RD maps at the previous time instants carry relevant information and will improve the performance of the interference mitigation when taken into account. Hence, the input in Radar-SACAE, $S_{in} \in \mathbb{C}^{3c\times h\times w}$, is a concatenation of the RD map inputs at time t, $t-1$, and $t-2$, with $c=1$, $h=128$, and $w=64$, where c, h, and w represent the input channel, height, and width of the RD map.

$$S_{\text{in}} = \text{concat}(S_{\text{IF}_t}, S_{\text{IF}_{t-1}}, S_{\text{IF}_{t-2}}). \tag{5}$$

Spatial attention combines the images across the channel dimension. In our work, we have uniquely combined the three channel input images to give a three channel output where the first layer represents the mean value, the second layer the maximum value, and the third layer the minimum value across the channel dimension, as shown in Equation 6 below:

$$S_{\text{pre}} = \text{concat}(S_{\text{in,mean}}, S_{\text{in,max}}, S_{\text{in,min}}), \tag{6}$$

where

$$S_{\text{in,mean}} = \frac{1}{3}\sum_{c=1}^{3} S_{\text{in}},$$
$$S_{\text{in,max}} = \max_{c}(S_{\text{in}}),$$
$$S_{\text{in,min}} = \min_{c}(S_{\text{in}}).$$

This is followed by a 1×1 convolution operation, also referred to as a Network-in-Network operation. The filter operation executes a weighted summation of each channel element and reduces the channel dimension from 3 to 1. The last step in the spatial attention block is a sigmoid activation.

The output of the spatial attention, $S_{sa} \in \mathbb{C}^{1\times h\times w}$ is shown in Equation 7 below:

$$S_{\text{sa}} = \gamma(\text{conv}_{1\times 1}(S_{\text{pre}})), \tag{7}$$

where γ represents the sigmoid operation $\gamma(x) = \frac{1}{1+e^{-x}}$.

B. Encoder Block

The input to the encoder block ($S_{enc_in} \in \mathbb{C}^{1\times h\times w}$) is the output of the spatial attention block (S_{sa}) multiplied by original RD map at time t in the format of element-wise product, referred to as Hadamard product. This maintains the height and width of the RD map but with different level of attention given to all the individual elements depending on the learning of the model. Recall we have peak targets and noise floors in the input RD map and we want to accentuate the peaks and simultaneously minimize the noise floors. Mathematically, the encoder input is

$$S_{\text{enc,in}} = S_{\text{sa}} \circ S_{\text{IF}_\text{t}}. \tag{8}$$

The next block in Radar-SACAE is the encoder block. A convolution operation with a 7×7 filter, stride = 2, and padding = 3 takes place. The output dimension is thus half of the input in both the height and width dimensions. The operation is done 16 times and stacked. Hence, the input channel size is 1 and the output channel size is 16 as shown in Figure 2. After the convolution is done, we carry out Batch Normalization (BN) followed by the use of Rectified Linear Unit (ReLU) activation. BN helps to prevent internal covariate shift and gradient propagation problems. The ReLU activation introduces non-linearity into the network and helps the model to learn complex patterns. The process is shown below

$$S_{\text{enc,out}} = \text{ReLU}(\text{BN}(\text{Conv}_{7\times 7}(S_{\text{enc,in}}))). \tag{9}$$

C. Decoder Block

The final block in Radar-SACAE is the decoder block. The input to the decoder is the output from the encoder, ($S_{enc,out} \in \mathbb{C}^{16\times h\times w}$). The operation consists of a convolution transpose using a 7×7 filter, a stride = 2, padding = 3, and out padding = 1. By so doing, the convolution transpose output is twice the input. This implies a restoration to the height and width of our original input. The input channel size of the decoder is 16 and the output channel is 1. The final step is the application of ReLU activation. The decoder operation is shown below:

$$\hat{S}_{\text{RD}} = \text{ReLU}(\text{ConvTranspose}_{7\times 7}(S_{\text{enc,out}})). \tag{10}$$

IV. Analysis Methodology

A. Dataset

One of the challenges in the field of interference mitigation is the availability of dataset [13]. It is difficult to acquire both the interfered and clean data in practice. However, if a purely synthetic data is used, it will not properly capture the noise and clutters in a real environment. To offer a solution, the authors in [9] released a data set that combined the real data provided by [10] with synthetic interferers generated using Matlab Radar Toolbox. This is the dataset that we have used in this study. The dataset in RaDICaL [10] are the victim signals. That dataset was gathered from an in-car mmWave radar, utilizing a model AWR1843 BOOST developed by Texas Instruments. The description of the victim data is given in Table I. The aggressor details are shown in Table II. Some of the details of this agressor are as follows:

- It is a single interference source whose parameters are selected from a uniformly distributed intervals as shown.
- The interference amplitude is modulated according to the Signal to Interference and Noise Ratio (SINR), ranging from -5 dB to 25 dB with a fixed step of 5 dB.
- The simulated interference signal is then generated using an FMCW sensor via MATLAB R2021b Radar Toolbox and merged with the victim signal following a predefined procedure.
- After generating the time-domain data, the RD map of the interfered signal is computed using a 2D-FFT with dimensions of 64 × 128.
- Similarly, a 2D-FFT is applied to the original signals to produce the RD map of the corresponding reference.

TABLE I: Parameters of the Victim Radar.

Parameter	Value
Carrier frequency [GHz]	77
Sweep bandwidth [MHz]	153.6
Frame rate [frames/s]	30
Max range [m]	62.45
Max velocity [m/s]	23.02
Samples per chirp	64
Range FFT points	64
Sweep duration [μs]	21.12
Sampling frequency [MHz]	12.5
ADC sampling window [μs]	5.12
Range resolution [m]	0.97
Velocity resolution	0.36
Chirps per frame	128
Doppler FFT points	128

TABLE II: Parameters of the Agressor Radar.

Parameter	Minimum	Maximum	Step
SINR [dB]	-5	25	5
Carrier frequency [GHz]	76.8	77.2	0.1
Sweep bandwidth [MHz]	120	400	-
Sweep duration [μs]	4	30	-
Interferer distance [m]	2	63	-
Interferer velocity [m/s]	-23.05	0	-

B. Performance Metrics

The aim of interference mitigation is to boost detection probability while avoiding distortions that could skew results. The authors in [14] provided the radar interference community with two metrics that can be used to evaluate the performance of interference mitigation schemes and ensure

systematic comparison: SINR and Error Vector Magnitude (EVM).

For a 2D RD map, SINR is the ratio of the average power of object peaks to the noise floor and is expressed as:

$$\mathrm{SINR} = 10\log_{10}\left(\frac{\frac{1}{N_O}\sum_{\{n,m\}\in O}|\hat{S}_{\mathrm{RD}}[n,m]|^2}{\frac{1}{N_N}\sum_{\{n,m\}\in N}|\hat{S}_{\mathrm{RD}}[n,m]|^2}\right), \quad (11)$$

where N is the set of noise cells. The EVM is the second metric defined as the magnitude of the error vector between the clean RD map and the interfered RD map. The smaller the EVM, the better the quality of the RD map relative to the clean version. It is expressed as:

$$\mathrm{EVM} = \frac{|S_{\mathrm{RD,clean}}[n_o,m_o] - \hat{S}_{\mathrm{RD}}[n_o,m_o]|}{|S_{\mathrm{RD,clean}}[n_o,m_o]|}, \quad (12)$$

with n_o and m_o representing the indices of the maximal peak value in the RD map.

C. Training Parameters

To train the model, the hyperparameters were optimized using ray tune [15]. We present an overview of the hyperparameters in Table III. To achieve a more reliable estimate of the model's performance and prevent overfitting, we used the K-fold cross validation. The dataset was split into training, validation, and testing, with 10% of the data used for testing and the remainder for training and validation. To ensure that the predicted RD map respects the statistical properties of the clean RD map, we introduced a customized regularization that takes into account the mean and standard deviation of the clean RD map. During training, the loss is calculated as follows:

$$\mathcal{L}(S_{\mathrm{RD,clean}},\hat{S}_{\mathrm{RD}}) = \frac{1}{N_A}\sum_{\{n,m\}\in A}\|S_{\mathrm{RD,clean}} - \hat{S}_{\mathrm{RD}}\|_2^2 + \lambda(\beta_1+\beta_2), \quad (13)$$

where A represents all points in the RD map, $\lambda = 0.1$ is a fixed regularization factor, and β_1/β_2 are the absolute differences between the mean/standard deviation of the clean RD map and the model output respectively:

$$\beta_1 = |\bar{S}_{\mathrm{RD,clean}} - \bar{\hat{S}}_{\mathrm{RD}}| \text{ and } \beta_2 = |\sigma(S_{\mathrm{RD,clean}}) - \sigma(\hat{S}_{\mathrm{RD}})|.$$

The benefit of introducing this customized regularization is that the output of the model respects the central tendency and dispersion of the clean RD map. In essence we maintain the distribution, do not increase the noise floor but simultaneously accentuate the peaks.

V. Results

In this article, we do not focus on the results achieved using legacy methods such as zeroing, IMAT [16], ramp filtering [17], etc. These have been exhaustively studied in the literature and the common theme in all is that deep learning methods outperform legacy methods. Hence, we put our focus on the results achieved by our proposed model in comparison to other deep learning models: Radar-STDA [9], RD RIS Model D [18], and MLP. The results are compared based on quantitative (SINR, EVM) metrics, qualitative evaluation, and computational complexity.

TABLE III: Training Parameters for Radar-SACAE.

Parameter	Value
Batch size	16
Learning rate	0.001
Learning rate decay	step
Step size	10
Step decrement ratio	0.9
Loss function	MSE
First Regularization	L2
Second Regularization	Customized (13)
Optimizer	Adam
Cross validation	K-Fold
Number of folds	5
Epochs per fold	30

TABLE IV: Performance of Radar-SACAE in Comparison to State-of-the-Art Models.

Parameter	SINR(dB)	EVM	No of multiplications
Ground Truth	18.28	0	-
Radar-SACAE	16.47	0.0403	8.1M
Radar-STDA	16.34	0.0810	447.2M
RD-RIS	15.82	0.1643	21.2M
MLP	15.81	0.1104	35.8M

A. Quantitative Evaluation

The first subsection presents the numerical results for our proposed Radar-SACAE as shown in Table IV. In terms of SINR, our proposed scheme slightly outperforms the Radar-STDA scheme. We see a 1.8 dB improvement in SINR compared to the RD-RIS and MLP schemes. EVM measures the similarity between the ground truth RD map and the interference mitigated RD map. The lower the EVM, the close the image is to the true label. We observe that our scheme has the lowest EVM while the RD-RIS scheme exhibited the highest EVM.

B. Computational Complexity

Inspired by [19], we calculate the computational complexity of our model relative to other state-of-the-art models. This analysis is done in terms of the number of real-valued multiplications in the models. The number of multiplications is similar to the number of additions but we focus on multiplications since it is computationally more expensive.

For a 2D convolution, as it is in this study, the number of multiplications is calculated as follows:

$$N_{\mathrm{MUL_1}} = F_1 \times F_2 \times C_{\mathrm{in}} \times M_1 \times M_2 \times C_{\mathrm{out}}, \quad (14)$$

where the kernel/filter size is $F_1 \times F_2$, the output size is $M_1 \times M_2$, and the number of input and output channels are C_{in} and C_{out} respectively. The calculation for the fully connected only network (MLP) is seen in (15). Moving from the ℓ-th to the $(\ell+1)$-th layer will require $J_\ell J_{\ell+1}$ multiplications for the linear transformation, where J signifies the number of neurons in the layer:

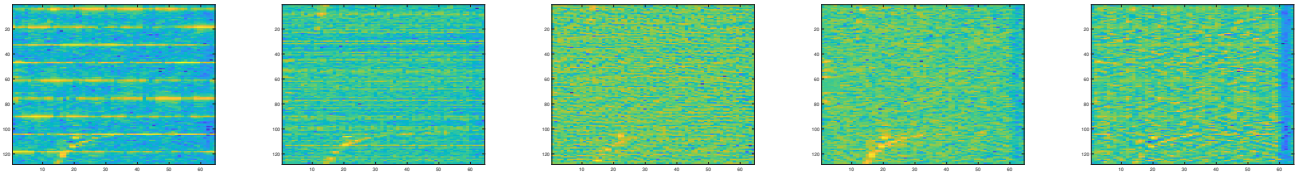

(a) Interference at t (b) Interference at t-1 (c) Interference at t-2 (d) Ground truth (e) Radar-SACAE

Fig. 3: Images of the RD Maps with Interference, without Interference and after Interference Mitigation using Radar-SACAE.

$$N_{\mathrm{MUL}_2} = \sum_{\ell=1}^{L} J_{\ell-1} J_{\ell}. \tag{15}$$

From Table IV, we can see that our proposed Radar-SACAE has the least computational complexity of all the considered models. The MLP and RD-RIS models require 4.4 times and 2.62 times more multiplications than Radar-SACAE respectively. Despite requiring more resources, these models are outperformed by Radar-SACAE in terms of SINR and EVM. The third state-of-the-Art model, Radar-STDA, requires 55.2 times more real-valued multiplications than our proposed model.

C. Qualitative Evaluation

Figure 3 shows the images of the RD map when using Radar-SACAE. The first three images are the RD maps with interference at time t, $t-1$, and $t-2$. Next, we see the ground truth and the RD map after interference mitigation using Radar-SACAE. We observe from Figure 3a that the RD map is noisy and the target peaks are buried. By using the RD maps in the two previous time instants, and leveraging on spatial attention, our proposed model is able to learn from previous RD maps and give more weight to the peak regions accordingly. This is in agreement with the work in [10] that previous RD maps carry useful information. The model is also more robust as it deals with interfernce and noise from more than once source.

VI. Conclusion

In this paper, we proposed a novel deep learning model (Radar-SACAE) to mitigate interference in FMCW radar based on spatial attention and convolutional autoencoder. This model uses the attention mechanism to learn from the spatial distribution of the current RD map and two previous RD maps. It then passes the result through a convolutional autoencoder. Our model outperforms other deep learning models in terms of SINR and EVM in addition to a highly significant gain in computational complexity. In the future work, we consider further reduction in computational complexity by adopting a hybrid approach which is a combination of traditional and deep learning methods.

References

[1] Z. Wei, H. Qu, Y. Wang, X. Yuan, H. Wu, Y. Du, K. Han, N. Zhang, and Z. Feng, "Integrated Sensing and Communication Signals Toward 5G-A and 6G: A Survey," *IEEE Internet of Things Journal*, vol. 10, no. 13, pp. 11 068–11 092, 2023.

[2] X. Cheng, D. Duan, S. Gao, and L. Yang, "Integrated Sensing and Communications (ISAC) for Vehicular Communication Networks (VCN)," *IEEE Internet of Things Journal*, vol. 9, no. 23, pp. 23 441–23 451, 2022.

[3] F. Liu, C. Masouros, A. P. Petropulu, H. Griffiths, and L. Hanzo, "Joint Radar and Communication Design: Applications, State-of-the-Art, and The Road Ahead," *IEEE Transactions on Communications*, vol. 68, no. 6, pp. 3834–3862, 2020.

[4] S. Rao, "Introduction to mmWave Sensing: FMCW Radars," *Texas Instruments (TI) mmWave Training Series*, pp. 1–11, 2017.

[5] A. Fuchs, J. Rock, M. Toth, P. Meissner, and F. Pernkopf, "Complex-Valued Convolutional Neural Networks for Enhanced Radar Signal Denoising and Interference Mitigation," in *2021 IEEE Radar Conference (RadarConf21)*. IEEE, 2021, pp. 1–6.

[6] M. Wagner, F. Sulejmani, A. Melzer, P. Meissner, and M. Huemer, "Threshold-Free Interference Cancellation Method for Automotive FMCW Radar Systems," in *2018 IEEE International Symposium on Circuits and Systems (ISCAS)*. IEEE, 2018, pp. 1–4.

[7] S. Lee, J.-Y. Lee, and S.-C. Kim, "Mutual Interference Suppression using Wavelet Denoising in Automotive FMCW Radar Systems," *IEEE Transactions on Intelligent Transportation Systems*, vol. 22, no. 2, pp. 887–897, 2019.

[8] J. Wang, "CFAR-based Interference Mitigation for FMCW Automotive Radar Systems," *IEEE Transactions on Intelligent Transportation Systems*, vol. 23, no. 8, pp. 12 229–12 238, 2021.

[9] L. Liu, R. Guan, F. Ma, J. Smith, and Y. Yue, "Radar-stda: A high-performance spatial-temporal denoising autoencoder for interference mitigation of fmcw radars," *IEEE Sensors Journal*, Jul. 2023.

[10] T.-Y. Lim, S. A. Markowitz, and M. N. Do, "RaDICaL: A Synchronized FMCW Radar, Depth, IMU and RGB Camera Data Dataset With Low-Level FMCW Radar Signals," *IEEE Journal of Selected Topics in Signal Processing*, vol. 15, no. 4, pp. 941–953, 2021.

[11] Y. Zigang and M. Anil, "Interference Mitigation For AWR/IWR Devices," in *Texas Instrument*, 2022, pp. 1–17.

[12] M.-H. Guo, T.-X. Xu, J.-J. Liu, Z.-N. Liu, P.-T. Jiang, T.-J. Mu, S.-H. Zhang, R. R. Martin, M.-M. Cheng, and S.-M. Hu, "Attention mechanisms in computer vision: A survey," *Computational Visual Media*, vol. 8, no. 3, pp. 331–368, Sep. 2022.

[13] T. Oyedare, V. K. Shah, D. J. Jakubisin, and J. H. Reed, "Interference suppression using deep learning: Current approaches and open challenges," *IEEE Access*, vol. 10, pp. 66 238–66 266, 2022.

[14] M. Toth, P. Meissner, A. Melzer, and K. Witrisal, "Performance comparison of mutual automotive radar interference mitigation algorithms," in *2019 IEEE Radar Conference (RadarConf)*, 2019, pp. 1–6.

[15] R. Liaw, E. Liang, R. Nishihara, P. Moritz, J. E. Gonzalez, and I. Stoica, "Tune: A research platform for distributed model selection and training," *arXiv preprint arXiv:1807.05118*, 2018.

[16] J. Bechter, F. Roos, M. Rahman, and C. Waldschmidt, "Automotive radar interference mitigation using a sparse sampling approach," in *2017 European Radar Conference (EURAD)*, 2017, pp. 90–93.

[17] M. Wagner, F. Sulejmani, A. Melzer, P. Meissner, and M. Huemer, "Threshold-Free Interference Cancellation Method for Automotive FMCW Radar Systems," in *2018 IEEE International Symposium on Circuits and Systems (ISCAS)*, 2018, pp. 1–4.

[18] J. Rock, M. Toth, E. Messner, P. Meissner, and F. Pernkopf, "Complex signal denoising and interference mitigation for automotive radar using convolutional neural networks," in *2019 22th International Conference on Information Fusion (FUSION)*, 2019, pp. 1–8.

[19] A. K. Gizzini, M. Chafii, A. Nimr, and G. Fettweis, "Deep Learning Based Channel Estimation Schemes for IEEE 802.11p Standard," *IEEE Access*, vol. 8, pp. 113 751–113 765, 2020.